

## Chapter 1.5.6

# SPECIAL METHODS OF WAVE DIFFRACTION

**D. Maystre, M. Saillard and G. Tayeb**

Laboratoire d'Optique Électromagnétique,  
UPRES A 6079,  
Centre National de la Recherche Scientifique Faculté des  
Sciences et Techniques de St Jérôme, Service 262,  
13397 Marseille Cedex 20,  
France

### E-M WAVES SCATTERING

#### Approximate and numerical methods

#### Contents

|    |  |    |
|----|--|----|
| §1 | Introduction   | 1  |
| §2 | Method of Fictitious Sources                               | 2  |
|    | Presentation of the Method                                 | 2  |
|    | A Canonical Problem  | 2  |
|    | Fictitious Sources and Basis Functions                     | 3  |
|    | Cylindrical and Bounded Scatterers                         | 4  |
| §3 | S-Matrix Method for Scattering by a Set of Bounded Objects | 7  |
|    | Theory   | 7  |
|    | Numerical Application                                      | 10 |
| §4 | Hybrid Methods for Surface and Volume Scattering           | 11 |
|    | Scattering by Randomly Rough Surfaces                      | 11 |
|    | Scattering by Rough Inhomogeneous Media                    | 14 |
| §5 | Conclusion   | 15 |

### §1. Introduction

Electromagnetic and acoustic waves have taken an increasing importance in modern technologies like electromagnetic and optical communications, imaging, object and surface characterisation, electronic and optical components and space astronomy. As a consequence, the development of accurate tools devoted to the numerical simulation of electromagnetic and acoustic waves scattering has a vital importance. In particular, the solution to problems of scattering from a disordered or periodic set of objects or from rough surfaces is necessary in the study of many phenomena of modern physics like weak and strong localization, or in many scientific and technological areas like sea or ground surface characterisation, photonic band structures, diffraction gratings and heterogeneous films. This chapter is devoted to the study of this kind of structure in the frame of **electromagnetic scattering**.

In many cases, one can consider that the waves are monochromatic. Some specific methods like finite-difference time-domain (FDTD) can be applied to wide-band signals, but for linear materials, a

monochromatic approach of scattering provides the solution to wide-band problems using Fourier transform. For this reason, this chapter is restricted to the case of monochromatic waves. We will concentrate on two-dimensional (2D) problems of scattering. These problems are much simpler than problems of scattering from 3D objects but the methods that will be presented can be extended to this more complicated case. It must be noted that the solution to 2D problems of scattering is not academic: in practice, many scattering objects are nearly 2D.

From our experience, it turns out that the solution to a wide class of scattering problems cannot be achieved from the use of a unique and universal numerical tool. In general, a better way to deal with a large class of problems is to have a set of numerical programs available, each of them being well adapted to a special kind of problem. In this chapter, some of them will be described. They are characterised by their robustness and precision, and they lead to the solution of a linear system of equations.

Very often, the efficiency of a numerical method for solving a scattering problem is closely linked to the representation of the fields on adequate bases. It allows a reduction of the size of the linear system to be inverted, thus a reduction of the computation time and memory storage. The fictitious sources method is a typical example of this rule, where the structure reduces to a single piecewise homogeneous scattering object. Closely related to the integral method, it allows one to escape from the problems encountered with singularities of the kernels thanks to a judicious representation of the fields from the use of fictitious sources placed apart from the surface of the scatterer. The precision of the results can be estimated very easily from a numerical test.

The notion of  $S$  matrix of a single scatterer enables one to solve the problem of diffraction from an arbitrary set of homogeneous objects through the use of the  $S$ -matrix method. This method fully takes into account the coupling between the objects from multiple scattering and can deal with a large number of scattering objects.

Finally, a solution to the more complex problem where the scattering objects are located below a rough surface separating two dielectric materials is presented. In that case, a hybrid method combining an integral theory for the rough surface, a fictitious sources method (or a classical integral theory) for each scatterer and an S-matrix method for the coupling between the set of objects is described. A vital factor of the efficiency of this method lies on the use of an integral equation with only one unknown function. This kind of integral equation allows one to save memory storage and thus to take into account a large number of scatterers.

Through the whole chapter, an orthogonal coordinate system with unit vectors  $\hat{x}, \hat{y}, \hat{z}$  is used. In the case of 2D problems,  $\hat{z}$  will give the invariance direction. Time-harmonic fields are represented by complex vectors using a time dependence in  $\exp(-i\omega t)$ . We denote by  $\epsilon_0$  and  $\mu_0$  the permittivity and the permeability of vacuum by  $k_0 = 2\pi/\lambda_0 = \omega(\epsilon_0 \mu_0)^{1/2}$  the wave number and by  $\eta_0 = (\mu_0/\epsilon_0)^{1/2}$  the vacuum impedance. The permeability is assumed to be  $\mu_0$  everywhere (non-magnetic materials).

## §2. Method of Fictitious Sources

### Presentation of the Method

The method of fictitious sources (MFS) is a versatile and reliable method able to deal with many scattering problems. It relies upon a simple idea: the electromagnetic field in the various domains of the diffracting structure is expressed as a combination of fields radiated by adequate electromagnetic sources. These sources have no physical existence, which is why they are called “fictitious” sources located in homogeneous regions and not on the interfaces. In other words, one can consider that they generate electromagnetic fields that faithfully map the actual field; thus they form a convenient basis for this field. From a numerical point of view, proper bases are those capable of representing the solution with the fewest number of functions. Obviously, the quality of the bases is closely linked with the nature of the sources and their location. The freedom in the choice of the sources provides a great adaptability to various complex problems.

The MFS has been developed in the Laboratoire d’Optique Électromagnétique in the past decade, both from theoretical and numerical points of view (Tayeb, 1990, 1994; Tayeb *et al.*, 1991; Cadilhac and Petit, 1992; Zolla, 1993; Petit and Zolla, 1994; Zolla *et al.*, 1994; Zolla and Petit, 1996). Almost at the same time and independently, two other groups have worked on the same basic ideas (Leviatan and Boag, 1987; Boag

*et al.*, 1988, 1989, 1993; Hafner 1990, 1995), but their approaches are different from ours. In fact, one of the first attempts at using this method is probably due to Kupradze (1967). Our approach relies on unquestionable theorems of functional analysis. For conciseness, this aspect is not developed here, but the interested reader can refer to Tayeb (1990) for gratings problems or Cadilhac and Petit (1992) for 3D and cylindrical scatterers.

### A Canonical Problem

In order to give a framework to the method, let us consider a 3D diffraction problem by a bounded homogeneous object whose boundary is a closed surface  $\mathcal{C}$  (Fig. 1). We assume that  $\mathcal{C}$  is of class  $C^2$ , and we denote by  $\hat{n}$  the unit vector of the outward normal. Note that the hypothesis of  $C^2$  surfaces is used to establish some mathematical properties (completeness of bases), but numerically the method still works if  $\mathcal{C}$  is piecewise twice differentiable. We call  $\Omega_1$  (resp.  $\Omega_2$ ) the exterior (resp. interior) of  $\mathcal{C}$ . The domain  $\Omega_1$  (resp.  $\Omega_2$ ) is filled with a material of permittivity  $\epsilon_1$  (resp.  $\epsilon_2$ ) that is positive (resp. complex with positive imaginary part). The object is illuminated by a known incident field  $F^{\text{inc}} = (\mathbf{E}^{\text{inc}}, \mathbf{H}^{\text{inc}})$ , and we look for the total field  $F = (\mathbf{E}, \mathbf{H})$ . Here,  $F$  and  $F^{\text{inc}}$  are short notations for the components of both electric and magnetic fields. From the Stratton–Chu formulae (Martin and Ola, 1993), it turns out that the electromagnetic field at any point can be deduced from the values of  $\hat{n} \times \mathbf{E}$  and  $\hat{n} \times \mathbf{H}$  on  $\mathcal{C}$ . That is why it is convenient to represent the field by the couple  $\Phi$  of vector functions defined on  $\mathcal{C}$ , which is the unknown of the problem

$$\Phi = (\hat{n} \times \mathbf{E}, \hat{n} \times \eta_0 \mathbf{H}). \quad (1)$$

In the same way, the incident field can be represented by the couple of functions  $\Phi^{\text{inc}}$  defined on  $\mathcal{C}$ :

$$\Phi^{\text{inc}} = (\hat{n} \times \mathbf{E}^{\text{inc}}, \hat{n} \times \eta_0 \mathbf{H}^{\text{inc}}). \quad (2)$$

We will also make use of the scattered field  $F^{\text{sc}}$ , defined as the difference between the actual total field and the incident field:

$$F^{\text{sc}} = F - F^{\text{inc}}. \quad (3)$$

The problem is to find the total field  $F$  such that:

- (a) the scattered field  $F^{\text{sc}}$  satisfies Maxwell’s equations in  $\Omega_1$  and a radiation condition at infinity,
- (b) the total field  $F$  satisfies Maxwell’s equations in  $\Omega_2$  and
- (c) the boundary conditions on the surface  $\mathcal{C}$  of the scatterer are fulfilled.

Let us consider sources  $S_{1,n}$  ( $n = 1, 2, \dots, N$ ) placed in  $\Omega_2$  and that radiate fields  $F_{1,n} = (\mathbf{E}_{1,n}, \mathbf{H}_{1,n})$  in the whole space supposed to be filled with the material of permittivity  $\epsilon_1$ . Note that since the sources are placed in  $\Omega_2$ ,  $F_{1,n}$  has no singularity in  $\Omega_1$ , and  $F_{1,n}$  verifies condition (a) above. A linear combination  $\sum_n c_{1,n} F_{1,n}$  of such fields will also fulfil condition (a) and, if  $c_{1,n}$

are well chosen, can be regarded as an approximation for  $F^{sc}$  in  $\Omega_1$ . In the same way, we consider sources  $S_{2,n}$  placed in  $\Omega_1$ , and radiating fields  $F_{2,n}$  in the whole space supposed to be filled with the material of permittivity  $\varepsilon_2$ . A linear combination  $\sum_n c_{2,n} F_{2,n}$  of such fields fulfils condition (b) and, if  $c_{2,n}$  are well chosen, can be regarded as an approximation for  $F$  in  $\Omega_2$ . Denoting by  $\Phi_{1,n}$  and  $\Phi_{2,n}$  the boundary values of the fields  $F_{1,n}$  and  $F_{2,n}$  on  $\mathcal{C}$ , the continuity of the tangential components of the total field on  $\mathcal{C}$  (condition (c)) reduces to

$$\Phi^{inc} + \sum_n c_{1,n} \Phi_{1,n} - \sum_n c_{2,n} \Phi_{2,n} = 0. \quad (4)$$

It is possible to define adequate vector spaces for the mathematical objects  $\Phi, \Phi^{inc}, \Phi_{1,n}$  and  $\Phi_{2,n}$ . From this point of view, the equation above may be understood as the decomposition of  $\Phi$  on two different total families (bases)  $\Phi_{1,n}$  and  $\Phi_{2,n}$  according to

$$\begin{aligned} \Phi &= \Phi^{inc} + \lim_{N \rightarrow \infty} \sum_{n=1}^N c_{1,n}(N) \Phi_{1,n} \\ &= \lim_{N \rightarrow \infty} \sum_{n=1}^N c_{2,n}(N) \Phi_{2,n}. \end{aligned} \quad (5)$$

The convergence notion in Eq. (5) is related to the scalar product (thus to the norm) defined in these vector spaces. Without going into detail, it is important to retain that the norm involves surface integrals on  $\mathcal{C}$  of the tangential components of the fields  $F^{inc}, F_{1,n}, F_{2,n}$  (i.e.,  $\Phi^{inc}, \Phi_{1,n}, \Phi_{2,n}$ ) and of their surface divergence on  $\mathcal{C}$ .

In the numerical implementation, the set of sources will be finite, and the associated families will not be total, which means that Eq. (4) cannot be exactly fulfilled. For a given finite number  $N$  of sources, the aim

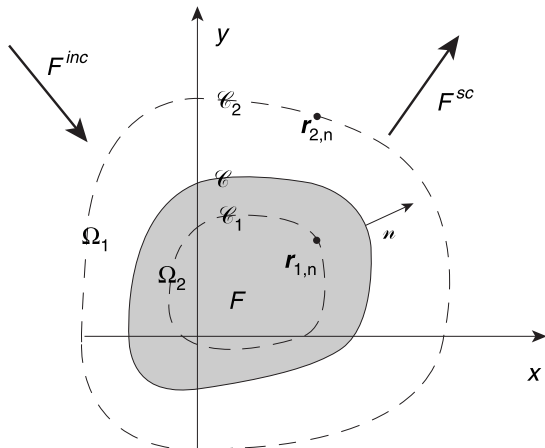
is to determine the coefficients  $c_{1,n}$  and  $c_{2,n}$  (depending on  $N$ ) that give the following norm its minimum value  $\Delta_N$ :

$$\begin{aligned} \Delta_N &= \min \left\| \Phi^{inc} + \sum_{n=1, N} c_{1,n}(N) \Phi_{1,n} \right. \\ &\quad \left. - \sum_{n=1, N} c_{2,n}(N) \Phi_{2,n} \right\|. \end{aligned} \quad (6)$$

Let us provide some remarks about the choice of this norm and the way of solving the problem.

- In some works (Leviatan and Boag, 1987; Boag *et al.*, 1988, 1989), the problem is solved from Eq. (4) with the help of a point matching method by enforcing the boundary condition (c) at some sampling points on  $\mathcal{C}$ . With a convenient choice of the number of these points (one should get a linear system with as many unknowns  $c_{1,n}$  and  $c_{2,n}$  as equations), it is possible to fulfil exactly the boundary condition at these points. But the boundary condition may be badly fulfilled between them, and strong oscillations of the left-hand side of (4) can be observed, which is why we suggest the improvement described in the next paragraph.
- If a least-squares algorithm is used in order to minimise the norm (6), the number of sampling points on  $\mathcal{C}$  can be increased independently of the number  $N$  of sources. Compared with the preceding method, we obtain a better accuracy for the same computation time.
- Keeping in the norm not only the tangential components of the fields but also their tangential derivatives (coming from the surface divergence contribution to the scalar product), the tangential variations are minimised as well, which ensures that the solution will not present strong and spurious oscillations between the sampling points. In fact, our numerical experiments have shown that these tangential derivative terms in the norm are useless in most problems, and can often be neglected.
- The least-squares minimisation process has another interesting feature. The normalised error  $\tilde{\Delta}_N = \Delta_N / \|\Phi^{inc}\|$  expresses the accuracy in the boundary condition (c) and provides a good criterion on the precision of the solution. This feature is very useful from a practical point of view and enables one to avoid time-consuming convergence tests.

**Figure 1** The scatterer is the greyed region with surface  $\mathcal{C}$ , interior  $\Omega_2$ , and exterior  $\Omega_1$ . The general idea is to express the scattered field  $F^{sc}$  in  $\Omega_1$  as a combination of fields radiated by sources lying in  $\Omega_2$ , and the total field  $F$  in  $\Omega_2$  as a combination of fields radiated by sources lying in  $\Omega_1$ .



As soon as the best coefficients  $c_{1,n}$  and  $c_{2,n}$  are obtained, the field in each region is given by

$$F^{\text{sc}} \approx \sum_{n=1, N} c_{1,n} F_{1,n} \quad \text{in } \Omega_1, \quad (7)$$

$$F \approx \sum_{n=1, N} c_{2,n} F_{2,n} \quad \text{in } \Omega_2. \quad (8)$$

The case of an infinitely conducting body can be treated in the same way. Obviously, coefficients  $c_{2,n}$  vanish, condition (b) is cancelled and condition (c) is replaced by the vanishing of the tangential components of the electric field on  $\mathcal{C}$ . The scattered field is obtained by minimising on  $\mathcal{C}$  the norm

$$\left\| \hat{\mathbf{n}} \times \mathbf{E}^{\text{inc}} + \sum_{n=1, N} c_{1,n} (N) \hat{\mathbf{n}} \times \mathbf{E}_{1,n} \right\|.$$

### Fictitious Sources and Basis Functions

The choice of the sources has a vital influence on the performance of the MFS. The Israeli group (Leviatan and Boag, 1987; Boag *et al.*, 1988, 1989, 1993) uses patch-currents (3D problems) or strip-currents (2D problems), whereas multipoles are used in Hafner's work (1990, 1995). In our studies, we have focussed on 2D problems: diffraction by a rod (or a set of rods), and diffraction by a grating. For each of these problems, we have tested two kinds of sources for which we have demonstrated the completeness of the associated bases  $\Phi_{1,n}$  and  $\Phi_{2,n}$ . These two kinds of sources are called "wire sources" or "sheet sources", and are described in the following section. Both provide reliable numerical solutions.

### Cylindrical and Bounded Scatterers

**Presentation of the Problem** In this section, the scatterer is a rod of infinite length or a set of such rods (Fig. 2). The extension of the theory to problems with more than one scatterer requires some mathematical prerequisites, but from a numerical point of view, this extension is straightforward. The total field in each bounded medium is represented as a combination of fields radiated by sources placed outside this medium. The same remark holds for the scattered field in the unbounded medium. The boundary conditions are matched on the discontinuity surfaces by mean of a least-squares minimisation. More details and examples on this subject can be found in Zolla *et al.* (1994).

For the sake of simplicity, we consider the diffraction by one homogeneous rod in a classical 2D ( $z$ -independent) problem where the incident field is also  $z$ -independent (for conical diffraction see Petit and Zolla (1994)). In that case, the problem reduces to two independent problems: the  $s$ -polarisation case where the electric field is parallel to the  $z$  axis, and the  $p$ -polarisation case where the magnetic field is paral-

lel to the  $z$  axis. Each of these cases leads to a scalar problem where the unknown  $u$  is the  $z$  component of either  $\mathbf{E}$  ( $s$  polarisation) or  $\mathbf{H}$  ( $p$ -polarisation):

$$u = \begin{cases} E_z & \text{in } s\text{-polarisation} \\ H_z & \text{in } p\text{-polarisation.} \end{cases} \quad (9)$$

**Choice of the Wire Sources and Solution of the Problem** We first focus on the determination of the basis elements  $\Phi_{1,n}$ . According to §2.2, the sources  $S_{1,n}$  are placed in  $\Omega_2$  and radiate in the whole space filled with a material of permittivity  $\epsilon_1$ . Let  $\mathcal{C}_1$  be a closed curve inside  $\mathcal{C}$  (see Fig. 1, assuming now that it is related to a 2D problem), and  $\mathbf{r}_{1,n}$  be the vector representation of a point on this curve. Denoting by  $v_j$  the optical index filling  $\Omega_j$ ,  $\epsilon_j = v_j^2$  the relative permittivity and  $k_j = k_0 v_j$  the wavenumber, the unique solution  $F_{1,n}(x, y)$  satisfying a radiation condition of the equation

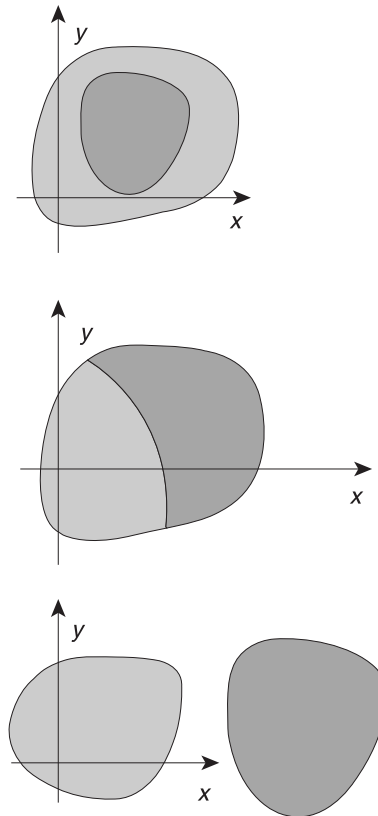
$$\Delta F_{1,n} + k_1^2 F_{1,n} = 4i \delta(\mathbf{r} - \mathbf{r}_{1,n}) \quad (10)$$

is the Hankel function

$$F_{1,n}(x, y) = H_0^{(1)}(k_1 \|\mathbf{r} - \mathbf{r}_{1,n}\|). \quad (11)$$

The source  $S_{1,n}$  (right-hand side of Eq. (10)) can be interpreted as a wire antenna located at  $\mathbf{r}_{1,n}$ , and we call it a "wire source". According to (1), the basis

**Figure 2** Three different cross sections in the case of two rods.



element  $\Phi_{1,n}$  contains the values on  $\mathcal{C}$  of the tangential field components and reduces here to a couple of scalar functions defined on  $\mathcal{C}$ , the other components being equal to 0,

$$\Phi_{1,n} = \left( F_{1,n}, \frac{i}{k_0} p_1 DF_{1,n} \right) \quad (12)$$

where  $DF_{1,n}$  stands for the normal derivative of  $F_{1,n}$  on  $\mathcal{C}$ , and  $p_j$  is a polarisation dependent constant:

$$p_j = \begin{cases} 1 & \text{for } s\text{-polarisation} \\ 1/\varepsilon_j & \text{for } p\text{-polarisation.} \end{cases} \quad (13)$$

The basis elements  $\Phi_{2,n}$  are constructed in the same way, but the sources  $S_{2,n}$  are now located at  $\mathbf{r}_{2,n}$  on a closed curve  $\mathcal{C}_2$  surrounding  $\mathcal{C}$ :

$$F_{2,n}(x, y) = H_0^{(1)}(k_2 \|\mathbf{r} - \mathbf{r}_{2,n}\|), \quad (14)$$

$$\Phi_{2,n} = \left( F_{2,n}, \frac{i}{k_0} p_2 DF_{2,n} \right). \quad (15)$$

The last problem is to determine an optimal location for the sources. Although it is proved (Cadilhac and Petit, 1992) that the solution converges towards the exact one when the number  $N$  of sources increases, it is important to place the sources in such a way that this convergence is fast. There is no absolute rule, but from our numerical experiments, good results are generally obtained when the distance between adjoining sources is about  $\lambda/10$ , as well as the distance from the sources to the surface  $\mathcal{C}$ . It is generally advisable to increase the density of sources near the regions where the radius of curvature of  $\mathcal{C}$  is smaller.

In this case, the scalar product between two couples  $\Phi = (u, v)$  and  $\Phi' = (u', v')$  is

$$(\Phi | \Phi') = \int_{\mathcal{C}} (u\bar{u}' + \partial_t u \partial_t \bar{u}' + v\bar{v}') d\varrho, \quad (16)$$

where  $\partial_t$  stands for the tangential derivative on  $\mathcal{C}$ , and  $\varrho$  is the curvilinear abscissa. As suggested in §2.2, some liberties can be taken in the numerical implementation, and the term  $\partial_t u \partial_t \bar{u}'$  can be suppressed without drawbacks.

The solving of the least-squares problem (6) gives the coefficients  $c_{1,n}$  and  $c_{2,n}$ , and thus the field can be computed everywhere using (7) and (8).

**Sheet Sources** These sources can be an alternative to the previous sources, where the basis functions  $\Phi_{1,n}$  are built from the solution satisfying a radiation condition of

$$\Delta F_{1,n} + k_1^2 F_{1,n} = f_{1,n} \delta_{\mathcal{C}_1}. \quad (17)$$

In our numerical works, the source  $S_{1,n}$  represented by the right-hand side of (17), whose support is  $\mathcal{C}_1$ , is chosen by setting  $f_{1,n}(\varrho_1) = f_{1,n}(M_1) = \exp(2i\pi p \varrho_1/L_1)$ , where  $\varrho_1$  is the curvilinear abscissa at a point  $M_1$  on  $\mathcal{C}_1$ ,  $L_1$  is the perimeter of

$\mathcal{C}_1$ , and the integer  $p = n - P - 1$  varies from  $-P$  to  $+P$  when  $n$  goes from 1 to  $N = 2P + 1$ . It can be shown (Cadilhac and Petit, 1992) that other sets of functions  $f_{1,n}$  can be used, provided that they form a total family  $L^2(\mathcal{C}_1)$ . The solution  $F_{1,n}(x, y) = F_{1,n}(M)$  is the convolution product

$$F_{1,n}(M) = \frac{1}{4i} \int_{\mathcal{C}_1} f_{1,n}(M_1) H_0^{(1)}(k_1 MM_1) dM_1. \quad (18)$$

The basis function  $\Phi_{1,n}$  is still obtained by (12). The functions  $\Phi_{2,n}$  are constructed in the same way, using sources  $S_{2,n} = f_{2,n} \delta_{\mathcal{C}_2}$  located on  $\mathcal{C}_2$ .

At a first glance, it could be thought that these sources require a greater numerical effort than the wire sources. In fact, using Gauss–Legendre quadrature to compute the convolution products, it comes out that the computation time remains on the same order, specially when the objects have smooth boundaries.

**S Matrix** It is often useful to characterise the diffraction properties of the rod by a *scattering matrix*  $\mathbf{S}$ . For this purpose, we consider a circle  $\mathcal{D}$  with radius  $R$  containing the entire rod (Fig. 3). Outside this circle, the  $z$  component  $u$  of the electromagnetic field satisfies the Helmholtz equation  $\Delta u + k_1^2 u = 0$ , and thus can be expanded in Fourier–Bessel series:

$$u(P) = \sum_{n=-\infty}^{+\infty} [a_n J_n(k_1 r) + b_n H_n^{(1)}(k_1 r)] \exp(in\theta). \quad (19)$$

In this series, the series with Hankel functions represents the field scattered by the rod, whereas the series with Bessel functions represents the incident field. Denoting by  $\mathbf{a}$  and  $\mathbf{b}$  the columns whose elements are  $a$  and  $b_n$ , the  $\mathbf{S}$  matrix links the incident and the diffracted field by

$$\mathbf{b} = \mathbf{S} \mathbf{a}. \quad (20)$$

In order to compute a truncated  $\mathbf{S}$  matrix with rank  $2M+1$ , we consider  $2M+1$  incident fields such as  $a_n = \delta_{m,n}$ :

$$\text{for } m = -M, M, \quad u_m^{\text{inc}}(P) = J_m(k_1 r) \exp(im\theta), \quad (21)$$

For each value of  $m$ , the diffraction problem is solved, and the scattered field  $u_m^{\text{sc}}(R, \theta) = \sum_{n=-\infty}^{+\infty} b_{m,n} H_n^{(1)}(k_1 R) \exp(in\theta)$  is calculated on the circle  $\mathcal{D}$ . A fast Fourier transform of this  $\theta$ -periodic function gives its  $2M+1$  central Fourier coefficients  $b_{m,n} H_n^{(1)}(k_1 R)$ , and thus the  $b_{m,n}$  (for  $n = -M, M$ ), which are nothing but the  $m$ th column of the  $\mathbf{S}$  matrix.

**Numerical Example** Let us consider (Fig. 4) a rod whose cross section is defined by the parametric equation  $x(t) = -0.5 + \cos t + \cos(2t)$ ,  $y(t) = \sin t + \sin(2t)/4$ . We place  $N$  wire sources on each profile  $\mathcal{C}_1$  and  $\mathcal{C}_2$ , and  $2N$  sample points on  $\mathcal{C}$  (these points are used in the numerical computation of the norm based on

Eq. (16)). This rod of index  $\nu_2 = 1.5$  lies in vacuum ( $\nu_1 = 1$ ) and is illuminated with an incidence  $\Theta^{inc} = 50^\circ$  by a plane wave with wavelength  $\lambda_0 = 1$ . Figure 5 gives the intensity scattered at infinity in the direction  $\theta$  (this function  $D(\theta)$  is precisely defined by Eq. (54)).

**Gratings** The MFS applies to diffraction gratings problems with very little changes. In the case of 1D gratings (we use the widespread notation that denotes by 1D grating or 1D rough surface a 2D object invariant towards the  $z$  direction) illuminated by a plane wave, the wire sources are replaced by a periodic distribution of wire sources with phase shifts related to the grating period and to the incident wave. The fields  $F_{1,n}$  and  $F_{2,n}$  are nothing but the well known Green's functions for gratings. More details can be found in Tayeb (1994), including hints for the computation of Green's function and several numerical examples.

In conclusion, the MFS can deal efficiently with many kinds of structures, including complex profile shapes. It is not plagued by the singularities problems encountered with classical integral methods, nor by the problems arising with integral methods in the case of objects covered with very thin layers (especially in the case of interpenetrating profiles, when it is not possible to get a closed form expansion of the fields between the layers), since only the free space Green's function (or the grating Green's function in case of periodic structures) is required. In our opinion, it is interesting from many points of view:

- Although its theoretical justification is based on difficult problems of functional

**Figure 3** Outside the circle  $\mathcal{C}$ , the field components expand in Fourier–Bessel series.

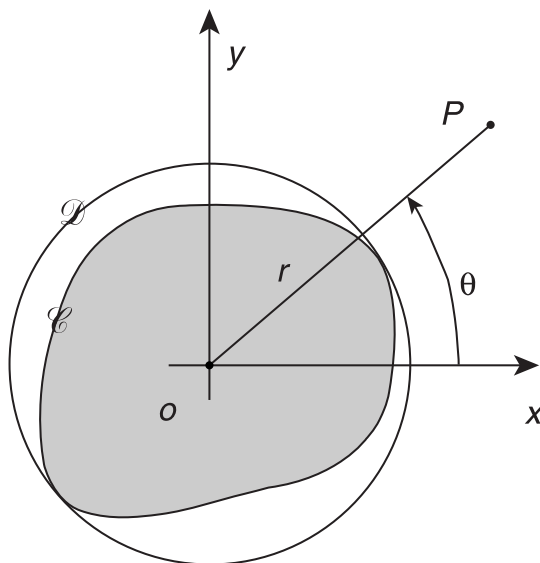


**Figure 4** Cross section of the rod and the two sets of wire sources ( $N=80$ ).

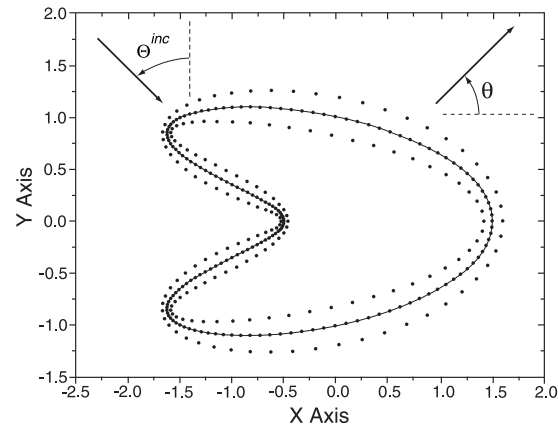
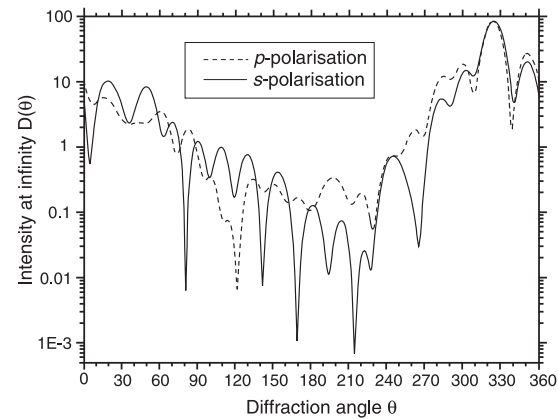


**Figure 5** Intensity at infinity for both polarisations.



analysis, its numerical implementation does not need solid mathematical background.

- The method includes the possibility of checking the accuracy of the results by means of the normalised error  $\tilde{\Delta}_N$ .
- Many adjustable parameters are available. For instance, we can choose the kind and the location of the fictitious sources, i.e., we can choose the basis functions for the representation of the fields.

This last feature makes the method powerful, but this freedom also leads to embarrassing choices. Basic rules can be picked out in order to automate the choice of the sources, and some work has been done in our laboratory along this line with wire sources. Without doubt, the performances of the MFS could be enhanced by the combination of various kinds of sources.

### §3. S-Matrix Method for Scattering by a Set of Bounded Objects

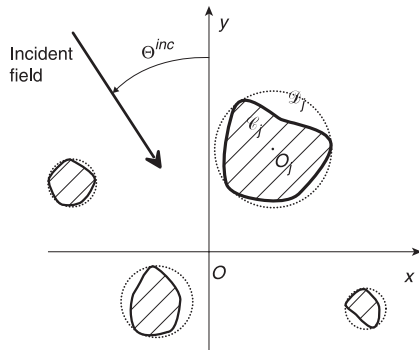
A theory of scattering by a finite set of diffracting objects arbitrarily distributed in a given region of space is presented in this section. This rigorous theory assumes a prior calculation of the scattering matrix of each object and, after a full handling of the coupling phenomena, leads to the inversion of a linear system of equations. In the following, it will be called the “S-matrix method”. Even though a pioneering theoretical work in that direction was achieved in electrostatics by Lord Rayleigh (1892) at the end of 19th century, it can be considered that the formalism described in this paper has been fully developed since the end of the 1980s by different groups working independently (Youssif and Köhler, 1988; Chew *et al.*, 1992; Elsherbeni and Kishk, 1992; Felbacq *et al.*, 1994; Nicorovici *et al.*, 1995; Vlassis *et al.*, 1996; Defos du Rau, 1997).

The published studies deal with 2D or 3D objects, arbitrary in shape or having simple geometries (circular cylinders or spheres), placed periodically or randomly in space, perfectly conducting or dielectric. Sometimes, the solution of the problem is carried out by a direct handling of all the scatterers and sometimes by increasing the number of the objects progressively through a recursive algorithm, but the basic features of the formalism remain similar. The first part of the section describes the theoretical approach where the objects are cylinders of arbitrary cross sections, followed by validation of the numerical implementation. Finally, a numerical application to the calculation of the transmission of light by a 2D photonic crystal will be shown.

#### Theory

Figure 6 shows the cross-section plane of a set of  $N$  parallel cylinders of boundaries  $\mathcal{C}_j (j = 1, 2, \dots, N)$  and interior domain  $\Omega_j$  lying in vacuum. In the following

**Figure 6** Description of the scattering problem and notations



and for the sake of simplicity, the cylinders are numbered from 1 to  $N$ , as opposed to the notations of §2. Each of these cylinders has a permittivity  $\epsilon_j = v_j^2$ ,  $\mathcal{C}_j$  being included in a circle  $\mathcal{D}_j$  of centre  $O_j$  and radius  $R_j$ . It is assumed that two arbitrary circles  $\mathcal{D}_j$  and  $\mathcal{D}_l$  have no intersection. For the sake of simplicity, the theory will be described for an s-polarised field incident upon metallic or dielectric (nonmagnetic) cylinders, with the electric field parallel to the  $z$  axis, but the generalisation to  $p$ -polarisation and to magnetic or perfectly conducting materials does not present any difficulty.

The incident electric field is given by

$$\mathbf{E}^{\text{inc}} = E^{\text{inc}} \hat{\mathbf{z}} \quad (22)$$

with

$$E^{\text{inc}} = \exp(ik_0(x \sin^{\Theta_{\text{inc}}} - y \cos^{\Theta_{\text{inc}}})) \quad (23)$$

The component on the  $z$  axis of the total electric field satisfies, in the sense of distributions, the Helmholtz equation

$$\Delta E + \tilde{k}^2(M)E = 0 \quad (24)$$

with

$$\tilde{k}^2(M) = k_0^2 \tilde{\epsilon}(M) = \begin{cases} k_0^2 \epsilon_j & \text{if } M \in \Omega_j \ (j = 1, 2, \dots, N) \\ k_0^2 & \text{if } M \notin \Omega_j \ (j = 1, 2, \dots, N), \end{cases} \quad (25)$$

$M$  being an arbitrary point in the space of coordinates  $(x, y)$ .

Let us rewrite this Helmholtz equation in the form

$$\Delta E + k_0^2 E = (k_0^2 - \tilde{k}^2(M))E \quad (26)$$

Bearing in mind that the incident field satisfies the Helmholtz equation  $\Delta E^{\text{inc}} + k_0^2 E^{\text{inc}} = 0$ , it can be derived from Eq. (26) that the scattered field  $E^{\text{sc}}$ , defined at any point of space as the difference between the total and incident fields, satisfies the equation

$$\Delta E^{\text{sc}} + k_0^2 E^{\text{sc}} = (k_0^2 - \tilde{k}^2(M))E \quad (27)$$

Hence, the scattered field at any point  $P$  of space outside the cylinders can be expressed using Green's theorem

$$E^{\text{sc}}(P) = -\frac{i}{4} k_0^2 \int \int H_0^{(1)}(k_0 PM) \times (1 - \tilde{\epsilon}(M)) E(M) dx dy \quad (28)$$

Let us note that the integral on the right-hand side of Eq. (28) can be restricted to the set of cylinders  $\Omega_j$  since  $k_0^2 - \tilde{k}^2(M)$  vanishes outside these cylinders. Consequently, the scattered field can be represented as a sum of integrals on the cylinders

$$E^{\text{sc}}(P) = \sum_{j=1, 2, \dots, N} E_j^{\text{sc}}(P) \quad (29)$$

$$E_j^{\text{sc}}(P) = \frac{i k_0^2 (\epsilon_j - 1)}{4} \int \int_{\Omega_j} H_0^{(1)}(k_0 PM) \times E(M) dx dy \quad (30)$$

By definition,  $E_j^{\text{sc}}(P)$  will be called ‘‘field scattered by the  $j$ th cylinder’’. This field can be expressed in a simpler form by considering (Fig. 7) the system of polar coordinates linked to the  $j$ th cylinder, with origin  $O_j$ ,  $\theta_j(P)$  and  $r_j(P)$  denoting the polar angle of  $P$  and its distance to  $O_j$ . Using Graf’s formula (Abramowitz and Stegun, 1970) for the Hankel function, it turns out that, if  $r_j(M) \leq r_j(P)$ ,

$$H_0^{(1)}(k_0 PM) = \sum_{m=-\infty}^{+\infty} \exp(-im\theta_j(M)) J_m(k_0 r_j(M)) \times H_m^{(1)}(k_0 r_j(P)) \exp(im\theta_j(P)). \quad (31)$$

and thus, Eq. (30) yields,  $\forall P$  such that  $r_j(P) \geq R_j$ ,

$$E_j^{\text{sc}}(P) = \sum_{m=-\infty}^{+\infty} b_{j,m} H_m^{(1)}(k_0 r_j(P)) \exp(im\theta_j(P)) \quad (32)$$

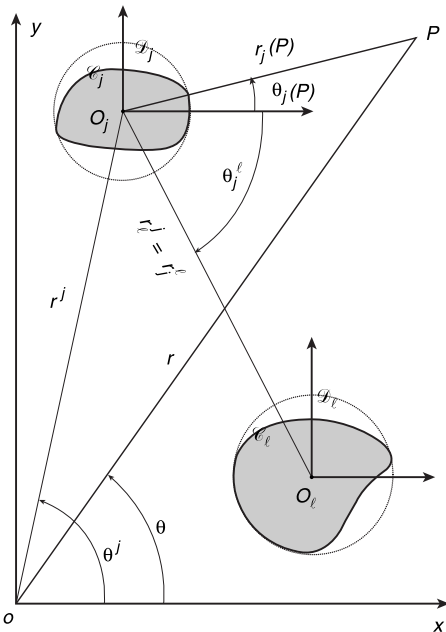
$$b_{j,m} = \frac{ik_0^2(\epsilon_j - 1)}{4} \iint_{\Omega_j} \exp(-im\theta_j(M)) \times J_m(k_0 r_j(M)) E(M) dx dy. \quad (33)$$

Finally, Eqs. (29) and (32) provide a modal expansion of the scattered field at any point outside the cylinders

$$E^{\text{sc}}(P) = \sum_{j=1,2,\dots,N} \sum_{m=-\infty}^{+\infty} b_{j,m} H_m^{(1)}(k_0 r_j(P)) \times \exp(im\theta_j(P)). \quad (34)$$

It must be emphasised that the existence of a modal expression of the field scattered by an arbitrary cylinder provided by Eq. (32) is quite general and extends

**Figure 7** Notations used for a change of coordinate system for Bessel functions. The subscripts refer to the system of coordinates linked to a given cylinder.



to any kind of material (dielectric, metallic, magnetic, perfectly conducting, etc.), regardless of the incident polarisation ( $p$  or  $s$ ). Even though this remark does not hold for Eq. (33), it can be considered that what follows is quite general since Eq. (33) will not be used any more.

Equation (34) expresses the scattered field from the polar coordinates of  $P$  in the  $N$  coordinates systems linked to the cylinders. In order to obtain an expression of this field in a unique system of coordinates, for instance the system linked to  $\mathcal{C}_\ell$ , we express the right-hand side of Eq. (32) in the  $\ell$ th coordinates system using Graf’s formula and the notations of Fig. 7: if  $r_\ell(P) \leq r_\ell^j = O_\ell O_j$ , then

$$H_m^{(1)}(k_0 r_j(P)) \exp(im\theta_j(P)) = \sum_{q=-\infty}^{+\infty} \exp(i(m-q)\theta_\ell^j) \times H_{q-m}^{(1)}(k_0 r_\ell^j) J_q(k_0 r_\ell(P)) \exp(iq\theta_\ell(P)), \quad (35)$$

which entails that Eq. (32) becomes,  $\forall P$  such that  $r_\ell(P) \leq r_\ell^j - R_j$ ,

$$E_j^{\text{sc}}(P) = \sum_{m=-\infty}^{+\infty} b_{j,m} \sum_{q=-\infty}^{+\infty} \exp(i(m-q)\theta_\ell^j) \times H_{q-m}^{(1)}(k_0 r_\ell^j) J_q(k_0 r_\ell(P)) \exp(iq\theta_\ell(P)). \quad (36)$$

The incident field given by Eq. (22) can be written in the same form

$$E^{\text{inc}}(P) = \exp(ik_0 \cdot \text{OP}) = \exp(ik_0 \cdot (\text{OO}_\ell + \text{O}_\ell \text{P})) \\ = \exp(ik_0 r^\ell \sin(\Theta^{\text{inc}} - \theta^\ell)) \\ \times \exp(ik_0 r_\ell(P) \sin(\Theta^{\text{inc}} - \theta_\ell(P)), \quad (37)$$

and bearing in mind that

$$\exp(iz \sin(u)) = \sum_{n=-\infty}^{+\infty} J_n(z) \exp(inu), \quad (38)$$

it comes out from Eq. (37) that at any point  $P$  of space,

$$E^{\text{inc}}(P) = \exp(ik_0 r^\ell \sin(\Theta^{\text{inc}} - \theta^\ell)) \sum_{n=-\infty, +\infty} \exp(in\Theta^{\text{inc}}) \\ \times J_n(k_0 r_\ell(P)) \exp(-in\theta_\ell(P)). \quad (39)$$

By adding the expression of the incident field given by Eq. (39), the expression of the field scattered by the cylinders  $\mathcal{C}_j$  with  $j \neq \ell$  given by Eq. (36) and the expression of the field scattered by  $\mathcal{C}_\ell$  given by Eq. (32), we get a rigorous modal expansion of the field around  $\mathcal{C}_\ell$  if  $R_\ell \leq r_\ell(P) \leq \min_{j \neq \ell} (r_\ell^j - R_j)$ ,

$$E(P) = \sum_{m=-\infty, +\infty} a_{\ell,m} J_m(k_0 r_\ell(P)) \exp(im\theta_\ell(P)) \\ + \sum_{m=-\infty, +\infty} b_{\ell,m} H_m^{(1)}(k_0 r_\ell(P)) \exp(im\theta_\ell(P)), \quad (40)$$

$$a_{\ell,m} = (-1)^m \exp(ik_0 r^\ell \sin(\Theta^{\text{inc}} - \theta^\ell) - im\Theta^{\text{inc}}) \\ + \sum_{j \neq \ell} \sum_{q=-\infty, +\infty} b_{j,q} \exp(i(q-m)\theta_\ell^j) H_{m-q}^{(1)}(k_0 r_\ell^j). \quad (41)$$

In order to write the equation above in a matrix form, we denote by  $\mathbf{a}_\ell$  and  $\mathbf{b}_\ell$  the infinite column matrices of components  $a_{\ell,m}$  and  $b_{\ell,m}$

$$\mathbf{a}_\ell = \mathbf{Q}_\ell + \sum_{j \neq \ell} \mathbf{T}_{\ell,j} \mathbf{b}_j \quad (42)$$

with  $\mathbf{Q}_\ell$  the column matrix of  $m$ th element  $Q_{\ell,m}$  given by

$$Q_{\ell,m} = (-1)^m \exp(ik_0 r^\ell \sin(\Theta^{\text{inc}} - \theta^\ell) - im\Theta^{\text{inc}}) \quad (43)$$

and  $\mathbf{T}_{\ell,j}$  a square matrix of  $(m, q)$ -th element  $T_{\ell,j,m,q}$  given by

$$T_{\ell,j,m,q} = \exp(i(q-m)\theta_\ell^j) H_{m-q}^{(1)}(k_0 r_\ell^j). \quad (44)$$

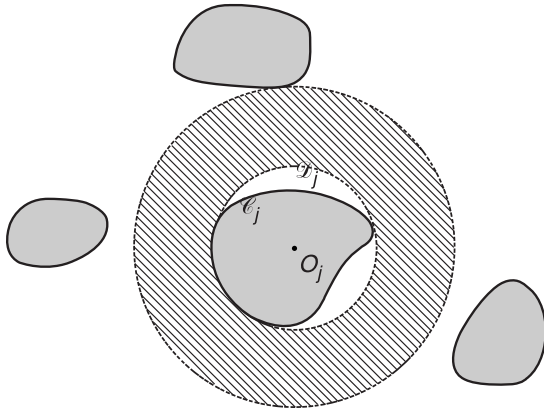
The well-known result stated in Eq. (40) is schematised in Fig. 8: the field around  $\mathcal{C}_j$  can be represented by a Fourier–Bessel modal expansion in the dashed annulus located between  $D_j$  and the circle of centre  $O_j$  passing through the closest point of the other cylinders (Suratteau and Petit, 1984). The authors of this paper have used this property to solve the problem of scattering by a grating of circular cylinders under some conditions.

Let us point out that the two series on the right-hand side of Eq. (40) are quite different from a physical point of view. The first, the coefficients of which are given by Eq. (41), represents the locally incident field, viz., the sum of the actual incident field and the field generated by the other cylinders in the direction of the  $\ell$ th cylinder, thus acting like secondary incident fields for this cylinder. On the other hand, the second term is the field scattered by the  $\ell$ th cylinder. As stated in §2, the coefficients of the scattered field and those of the locally incident field are linked by a matrix relation dependent on the parameters of the  $\ell$ th cylinder only

$$\mathbf{b}_\ell = \mathbf{S}_\ell \mathbf{a}_\ell, \quad (45)$$

where  $\mathbf{S}_\ell$  is an infinite square matrix.

**Figure 8** Domain of validity of the Fourier–Bessel expansion of the total field around one cylinder.



After multiplying Eq. (42) by  $\mathbf{S}_\ell$ , then using Eq. (45) to express the left-hand side, we eliminate the matrices  $\mathbf{a}_\ell$ , and it comes out that

$$\mathbf{b}_\ell - \sum_{j \neq \ell} \mathbf{S}_\ell \mathbf{T}_{\ell,j} \mathbf{b}_j = \mathbf{S}_\ell \mathbf{Q}_\ell, \quad (46)$$

which may be written in the form

$$\begin{bmatrix} \mathbf{I} & -\mathbf{S}_1 \mathbf{T}_{1,2} & -\mathbf{S}_1 \mathbf{T}_{1,3} & \dots \\ -\mathbf{S}_2 \mathbf{T}_{2,1} & \mathbf{I} & -\mathbf{S}_2 \mathbf{T}_{2,3} & \dots \\ -\mathbf{S}_3 \mathbf{T}_{3,1} & -\mathbf{S}_3 \mathbf{T}_{3,2} & \mathbf{I} & \dots \\ \dots & \dots & \dots & \dots \\ \dots & \dots & \dots & \dots \end{bmatrix} \begin{bmatrix} \mathbf{b}_1 \\ \mathbf{b}_2 \\ \mathbf{b}_3 \\ \dots \\ \dots \end{bmatrix} = \begin{bmatrix} \mathbf{S}_1 \mathbf{Q}_1 \\ \mathbf{S}_2 \mathbf{Q}_2 \\ \mathbf{S}_3 \mathbf{Q}_3 \\ \dots \\ \dots \end{bmatrix}, \quad (47)$$

which is a linear system of equations,  $\mathbf{I}$  being the infinite unit matrix. If the square and column submatrices  $\mathbf{S}_\ell$ ,  $\mathbf{T}_{\ell,j}$  and  $\mathbf{b}_\ell$  are truncated in order to keep the indices  $m$  and  $q$  between  $-M$  and  $+M$  in Eqs. (40) and (41), the final size of the system to be inverted is equal to  $N(2M+1)$ .

Finally, let us express the scattered field at infinity from the column matrices  $\mathbf{b}_\ell$ . With this aim, let us consider the expression of the scattered field outside the cylinders given by Eq. (34). In order to express this scattered field in the system of coordinates  $xy$ , we use Graf's formula once more: if  $r \geq r^j$ ,

$$\begin{aligned} & H_m^{(1)}(k_0 r_j(P)) \exp(im\theta_j(P)) \\ &= \sum_{q=-\infty, +\infty} \exp(i(m-q)\theta^j) J_{q-m}(k_0 r^j) \\ & \quad \times H_q^{(1)}(k_0 r) \exp(iq\theta), \end{aligned} \quad (48)$$

where  $r$  and  $\theta$  are the polar coordinates of point  $P$  of space in the  $xy$  plane. With use of Eq. (48), Eq. (34) becomes, far from the cylinders,

$$E^{\text{sc}}(P) = \sum_{q=-\infty, +\infty} b_q H_q^{(1)}(k_0 r) \exp(iq\theta), \quad (49)$$

$$b_q = \sum_{j=1, N} \sum_{m=-\infty}^{+\infty} b_{j,m} \exp(i(m-q)\theta^j) J_{q-m}(k_0 r^j). \quad (50)$$

The field at infinity can be expressed in a simpler way using the asymptotic form of the Hankel function (Abramowitz and Stegun, 1970),

$$H_q^{(1)}(k_0 r) \approx \sqrt{\frac{2}{\pi k_0 r}} \exp(i(k_0 r - q\frac{\pi}{2} - \frac{\pi}{4})), \quad (51)$$

and Eq. (49) yields

$$E^{\text{sc}}(P) \approx g(\theta) \frac{\exp(ik_0 r)}{\sqrt{r}}, \quad (52)$$

$$\begin{aligned} g(\theta) &= \sqrt{\frac{2}{\pi k_0}} \exp(-i\frac{\pi}{4}) \sum_{q=-\infty, +\infty} b_q \\ & \quad \times \exp(-iq\frac{\pi}{2}) \exp(iq\theta). \end{aligned} \quad (53)$$

The intensity at infinity (or the bistatic differential cross section) is defined by

$$D(\theta) = 2\pi |g(\theta)|^2, \quad (54)$$

and for lossless cylinders, the energy balance criterion writes (Van Bladel, 1964)

$$\int_0^{2\pi} |g(\theta)|^2 d\theta + 2\sqrt{\lambda_0} \operatorname{Re} \left[ \exp(i\frac{\pi}{4}) g(\Theta^{\text{inc}} - \frac{\pi}{2}) \right] = 0. \quad (55)$$

### Numerical Application

The use of our formalism needs a prior solution to the problem of scattering by each cylinder. For circular cylinders, the scattering matrices  $S_\rho$  of Eq. (45) are obtained from the classical method when the Fourier–Bessel expansions of the fields inside and outside the cylinder are matched on the surface (Van Bladel, 1964). For arbitrary shapes, a rigorous finite-elements method on the boundary based on a single-integral equation (Maystre and Vincent, 1972) or the fictitious sources method described in §2 has been implemented. These methods provide very precise results (generally to within  $10^{-3}$ ) except at irregular frequencies. When the new formalism is used for many cylinders, we have implemented numerous classical tests of validity on the numerical results (convergence of the results when the number  $2M+1$  of terms in the Fourier–Bessel expansions increases, energy balance for lossless materials, reciprocity).

For example, Fig. 9a shows a scattering object made of seven perfectly conducting cylinders of various shapes whilst Fig. 9b gives the intensity of the scattered field for an s-polarised incident field with a null incidence angle and wavelength  $\lambda_0$ . The scattered intensity has been computed for three values of  $2M+1$  between  $\theta = 0^\circ$  and  $\theta = 180^\circ$  (the region  $180^\circ < \theta < 360^\circ$  has been removed from the curve since the scattered intensity is very large for  $\theta \approx 270^\circ$ ). A convergence is obtained above  $M = 9$ . For  $M = 9$  and 14, the energy balance criterion is satisfied to within  $10^{-4}$ . The computation time on an IBM RS/6000-560 with 30 MFlops was equal to 25 s for  $M = 9$ .

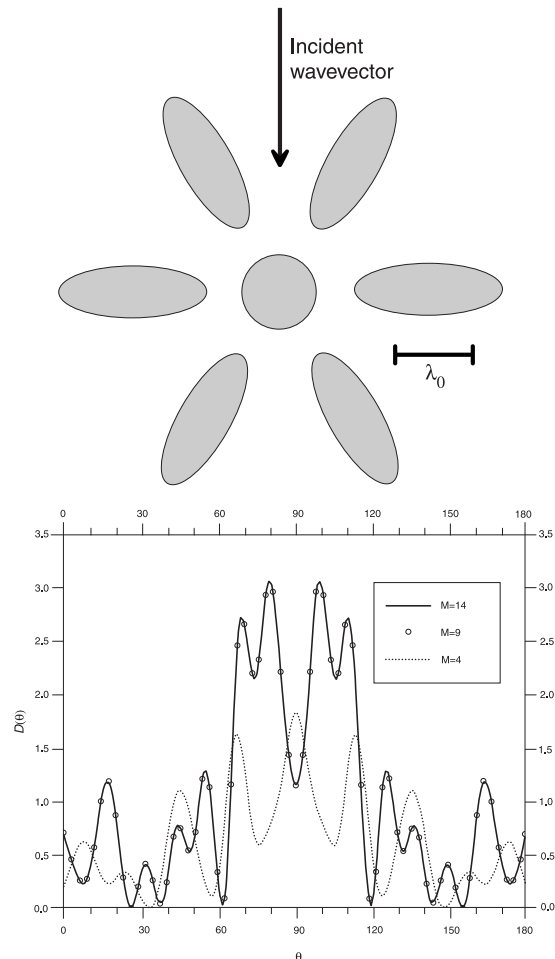
From these tests, it comes out that the precision remains about the same as that for a single cylinder, but of course the computation time increases with the number of cylinders since the size of the linear system to be solved increases with this number.

Finally, let us illustrate the capabilities of our computer code in the study of **photonic crystals**. Because of their periodicity, photonic crystals exhibit transmission gaps, which means that the field cannot propagate in such structures in a given range of frequencies, whatever the direction of propagation (Yablonoitch, 1994; Maystre, 1994; Joannopoulos,

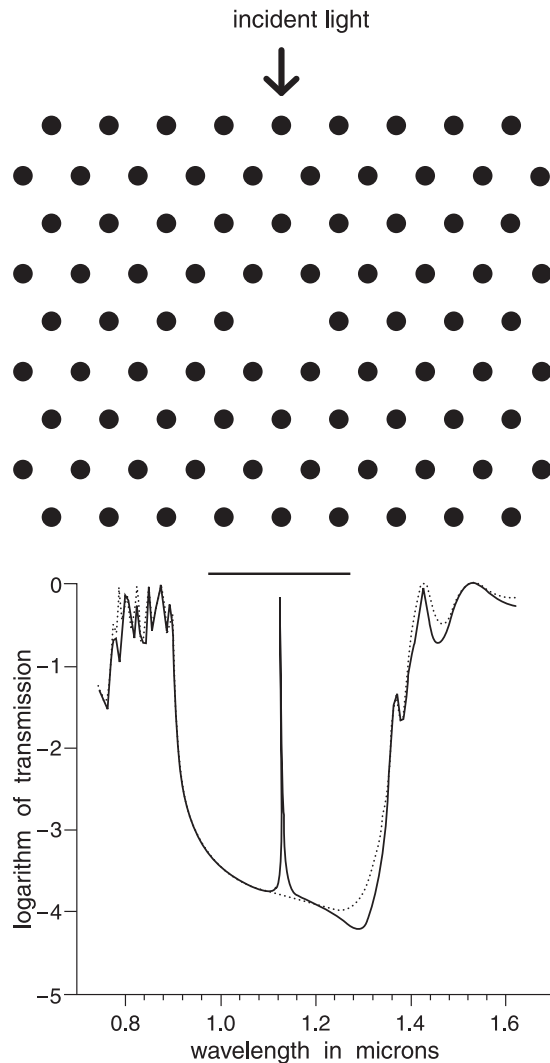
*et al.*, 1995; Nicorovici *et al.* 1995; Tayeb and Maystre, 1997). It is well known that the introduction of defects in the periodic lattice generates localized electromagnetic modes. Figure 10a shows a doped crystal, viz., a crystal with defects. This crystal is composed of a set of dielectric circular cylinders with radius  $R = 0.075 \mu\text{m}$ , spacing  $d = 0.5 \mu\text{m}$  (side of an elementary equilateral triangle) and optical index  $v = 2.9$ .

Figure 10b gives the decimal logarithm of the transmission of this crystal versus the wavelength. The incident field is a plane wave illuminating the crystal from the top of Fig. 10a. We compute the flux of the Poynting vector  $\Phi^{\text{trans}}$  for the total field on a segment located below the crystal (see Fig. 10a). We also compute the flux of the Poynting vector  $\Phi^{\text{inc}}$  for the incident plane wave only on the same segment. We

**Figure 9** Test of validity on a Scattering object. (a) Scattering object: the central circular cylinder has diameter  $\lambda_0$ , and the ellipses have large and small axes of  $2\lambda_0$  and  $2\lambda_0/3$  respectively. The centres of the circle and of one ellipse are separated by  $3\lambda_0$ . (b) Convergence of the intensity radiated by the scatterer shown in (a).



**Figure 10** Transmission by a photonic crystal. (a) Crystal with one defect. The segment below the structure is that used for the computation of the transmission. (b) Decimal logarithm of the transmission versus the wavelength for the crystal shown in (a) (solid curve) and for the same crystal, but with no defect (dotted curve).



define the transmission as  $T = \Phi^{\text{trans}} / \Phi^{\text{inc}}$ . Of course, the segment must be short enough since it must not collect the power flowing around the crystal. Figure 10b also gives the transmission for the same crystal as that of Fig. 10a, but without defect (dashed curve, the central cylinder has not been removed). The gap lies between wavelengths 0.9 and 1.35  $\mu\text{m}$ . When the central cylinder is removed (solid line), a sharp transmission peak appears at a wavelength  $\lambda_0 \approx 1.13 \mu\text{m}$ . This is due to the fact that, at this wavelength, a resonance occurs in the microcavity made by the defect, this microcavity playing the role of a relay for photons.

The method is specially adequate for the study of doped or nondoped photonic crystals. It is also a very

adequate tool in the study of the phenomenon of enhanced backscattering by a random set of rods arbitrarily shaped [Felbacq *et al.*, 1994]. Many other domains of investigation can be studied as well, in particular scattering by **random structures**, for instance, studies of Anderson localisation of light by a random set of cylinders.

#### §4. Hybrid Methods for Surface and Volume Scattering

In §3, it has been shown that methods based on a Fourier expansion of the scattered field, associated with addition theorems for cylindrical harmonics, are very efficient to deal with volume scattering. On the other hand, boundary integral methods are well suited for surface scattering. Therefore, in order to solve problems involving both *surface and volume scattering*, we present here an hybrid method that combines both integral and S-matrix formalisms. As a first step, we focus on the surface scattering problem alone, and we show that, even in that case, combining space and spectral representations may be helpful in the case of long-range interactions.

##### Scattering by Randomly Rough Surfaces

This topic has been extensively studied, for a wide range of applications, like remote sensing (Tsang *et al.*, 1985), nondestructive testing in optics (Goodman, 1975) and characterisation of materials with X-rays (Daillant and Gibaud, 1999). Our aim here is not to review the various methods devoted to this problem but to focus on a very efficient rigorous one, namely the boundary integral method.

**Modélisation of the Problem** Let us define a randomly *rough surface* as an infinite, flat on average, surface with random perturbation. In the following, only stationary surfaces are considered, and the distribution of heights is assumed to be a Gaussian distribution with zero mean. In this case, the roughness can be characterised either by an autocorrelation function  $C(\mathbf{r} - \mathbf{r}')$  or by its Fourier transform, the spectral density  $S(\mathbf{K})$ . The height of the roughness is described by the rms height  $\sigma = \sqrt{C(0)}$ .

As opposed to gratings, there is no periodicity here to allow the spatial restriction of the scattering problem to a finite area, but such a restriction is mandatory for numerical implementation. To overcome this problem, several approaches have been suggested:

(a) assume a periodic roughness with large periodicity compared to the incident wavelength and to a characteristic horizontal scale of the roughness (if it exists) (Maradudin *et al.*, 1989),

(b) restrict the random perturbation of the mean plane to a finite area (Maystre, 1983; Soto-Crespo and Nieto-Vesperinas, 1989) or

(c) use a finite beam as an incident wave (Saillard and Maystre, 1988).

With the aim of modelling as well as possible an actual experiment, we use Gaussian beams together with a beam simulation method (Saillard and Maystre, 1988) that permits us to synthesise beams with arbitrary size. Therefore, the problem reduces to the solution to the basic scattering problem of a narrow beam by an infinite rough interface. Due to the shape of the incident wave, the field on the surface must vanish at infinity, and the problem can be restricted to a finite area with negligible loss of accuracy. Of course the size of this area is linked to the shape of the beam, but also to the radius of interaction. If two points on the surface are separated by more than this distance, a change of the surface profile or of the incident field at one of them has negligible effects on the field at the other point. The radius of interaction depends on the incidence angle, on the polarisation, on the geometrical parameters of the surface and on the electromagnetic constants. In the resonance domain, for nongrazing incidence, the radius of interaction does not exceed a few wavelengths (Maystre, 1983), and in general, the scattering problem can be handled with the help of a **rigorous numerical method**. On the other hand, long-range interactions may occur in case of large scales of roughness (Torrance and Sparrow, 1967), when surface waves can propagate with low damping (Saillard and De Santo, 1996), or under grazing incidence (Brown, 1998, and references herein).

In this section, it is assumed that the rough interface separates two semi-infinite homogeneous media. In such problems, it can be shown, thanks to Green's theorem, that the scattered field can be derived from a surface density by integration on the boundary (Colton and Kress, 1983). Solving the scattering problem can thus be reduced to the determination of an unknown surface density, and numerical methods based on this result only require the discretisation of a surface. This is a large advantage, compared to volume integral methods or finite difference in the time domain (Hastings *et al.*, 1995), more general but heavier from a numerical point of view. As a consequence, boundary integral methods have become very popular in the field of rough surface scattering.

**Boundary Integral Methods** Let us consider a 1D rough surface  $\mathcal{C}$  described by a twice differentiable function  $y = \xi(x)$ . The complex permittivity is equal to  $\varepsilon$  if  $y > \xi(x)$  and  $\varepsilon_1$  in the lower half-space if  $y < \xi(x)$ . The domains filled with media of permittiv-

ities  $\varepsilon$  and  $\varepsilon_1$  are denoted by  $\Omega$  and  $\Omega_1$ , respectively. A local direct orthogonal basis  $(\hat{\mathbf{t}}, \hat{\mathbf{n}}, \hat{\mathbf{z}})$  is defined at each point on the surface, where the three unit vectors denote the tangential, the normal (toward  $\Omega$ ) and the  $z$ -axis directions respectively. The incident field is represented by either an  $s$ - or  $p$ -polarised monochromatic Gaussian beam, coming from  $y = +\infty$ . Denoting by  $u^{\text{inc}}$  either the electric or the magnetic incident field, depending on whether the polarisation is  $s$  or  $p$ , we have

$$u^{\text{inc}}(x, y) = \int_{-\infty}^{+\infty} P(\alpha - \alpha_0) \exp[i\alpha x - i\beta(\alpha)y] d\alpha \quad (56)$$

$$P(\alpha) = w \exp(-w^2 \alpha^2 / 2) \quad (57)$$

$$\alpha_0 = k \sin \Theta^{\text{inc}} \quad (58)$$

$$\beta = (k^2 - \alpha^2)^{1/2}, \quad \text{Im}(\beta) \geq 0. \quad (59)$$

The beam waist  $w$  and the mean angle of incidence  $\Theta^{\text{inc}}$  characterise the incident beam, and  $k$  represents the wavenumber in the upper medium. Let us write the scattered field at  $P$  in the upper medium as a single-layer potential with surface density  $\phi$  (Maystre and Vincent, 1972; Martin and Ola, 1993):

$$u^{\text{sc}}(P) = \int_{\mathcal{C}} G(P, M') \phi(M') ds', \quad (60)$$

where  $G$  denotes the 2D free space Green's function with wavenumber  $k$ .

Taking the limit of  $u^{\text{sc}}$  (Eq. (60)) and of its normal derivative when  $P$  goes to the boundary gives both the value of the field on the boundary and the outer limit of its normal derivative as a function of  $\phi$ :

$$u(M) = u^{\text{inc}}(M) + \int_{\mathcal{C}} G(M, M') \phi(M') ds', \quad (61)$$

$$\left( \frac{du}{dn} \right)_{\Omega} (M) = \frac{du^{\text{inc}}}{dn} (M) + \frac{1}{2} \phi + \int_{\mathcal{C}} \frac{dG}{dn} (M, M') \phi(M') ds'. \quad (62)$$

Then applying Kirchhoff-Helmholtz formula to the total field in  $\Omega_1$  and taking into account the boundary conditions ( $u_{\Omega} = u_{\Omega_1}$ ,  $(du/dn)_{\Omega_1} = q_1 (du/dn)_{\Omega}$  with  $q_1 = 1$  in  $s$ -polarisation and  $q_1 = \varepsilon_1/\varepsilon$  in  $p$ -polarisation) leads to the integral equation. Using an operator notation, viz., representing an integral operator by its kernel, we derive (Saillard and Maystre, 1990)

$$\left[ \left( \frac{\delta}{2} - \frac{dG_1}{dn'} \right) \mathbf{G} + q_1 \mathbf{G}_1 \left( \frac{\delta}{2} + \frac{dG}{dn'} \right) \right] \phi = - \left( \frac{\delta}{2} - \frac{dG_1}{dn'} \right) u^{\text{inc}} - q_1 \mathbf{G}_1 \frac{du^{\text{inc}}}{dn}. \quad (63)$$

As applied to bounded scatterers, such an integral equation does not ensure uniqueness of the solution

for the resonant frequencies of the associated interior Dirichlet problem. Since here the scatterer has infinite size, the spurious resonances do not occur, and using some combined field integral equation is not necessary.

Then Eq. (63) may be transformed into a set of linear equations with the help of a method of moments or a boundary finite-element method. Once the integral equation is solved, the scattering pattern at infinity is computed. Above the highest excursion of the surface profile, the scattered field can be written as a superposition of outgoing plane waves

$$u^{sc}(x, y) = \int_{-\infty}^{+\infty} B(\alpha) \exp[i\alpha x + i\beta(\alpha)y] d\alpha \quad (64)$$

with

$$B(\alpha) = \frac{-i}{4\pi\beta} \int \phi(x) \exp[-i\alpha x - i\beta(\alpha)\xi(x)] dx. \quad (65)$$

The differential reflection coefficient (DRC), which gives the part of the incident energy scattered into an angular interval  $\delta\Theta^{sc}$  around the scattering direction defined by the scattering angle  $\Theta^{sc} = (Oy, \mathbf{k}^{sc})$ , writes

$$\text{DRC} = \frac{|\beta(\alpha^{sc})B(\alpha^{sc})|^2}{P^{inc}}, \quad (66)$$

where  $\alpha^{sc} = k \sin \Theta^{sc}$  and  $P^{inc}$  is the total incident flux through a horizontal line:

$$P^{inc} = \int \beta(\alpha) |P(\alpha - \alpha_0)|^2 d\alpha, \quad (67)$$

With a method of moments, the size of the linear system results from the size of the sampled area, out of which  $\phi$  is assumed to be negligible. In some cases, it was observed that the surface density  $\phi$  decays very slowly away from the illuminated area, and another numerical method has been suggested to reduce the number of unknowns. It is illustrated here in the case of propagation of surface waves on metallic surfaces. It has also proven to be efficient under grazing incidence (Daillant and Gibaud, 1999).

**Surface Waves** The low decay of the unknown does not result from an inappropriate choice of the surface density, but involves some physical phenomenon, for instance propagation of *surface polaritons* along the boundary with metallic materials in optics. Indeed, since Wood anomalies on gratings have been observed (Wood, 1902), it is known that surface roughness can couple a *p*-polarised incident wave with surface plasmons on common metals like aluminium, silver or gold. In this case, the decay of the surface wave is governed by absorption in the metal and by scattering from surface roughness. For very rough surfaces, the damping only requires a few wavelengths, but for shallow surfaces, several tens of wavelengths

may be necessary. Therefore, the small perturbations method, taking multiple scattering of surface waves into account (Marvin and Celli, 1994), was used for very small heights, while the rigorous *integral formalism* combined with a moment method was restricted to deep surfaces. The aim of the method described consists in extending further the use of the boundary integral method down to the domain of validity of the perturbation theory.

The idea is quite simple. On a flat surface, a surface plasmon is a superposition of two plane waves travelling in opposite directions, thus requiring only two complex numbers for its description in the Fourier space. When a shallow random roughness is superimposed, the surface mode becomes localised (Maystre and Saillard, 1994), but its spatial extension is still large compared to the wavelength, and its spectral width, although finite now, remains small. Consequently, it is more convenient to use a Fourier basis to describe the surface density. On the other hand, the use of the beam simulation method to model accurately a true experiment requires localised test functions  $t_m$  for the integral equation, which is why this method is referred to as a coordinate-spectral method. This approach can be compared to the use of sheet sources in the MFS described in §2.

Since this problem concerns metallic surfaces, the high imaginary part of the refractive index makes the associated Green's function very narrow, permitting us to use the so-called impedance approximation, which consists in assuming a local relationship between the tangential electric and magnetic fields on the boundary, instead of an integral one. In this frame, Eq. (63) written in  $M(x, \xi(x))$  becomes

$$\begin{aligned} D_1(M)G\phi + q_1 N_1(M) \left( \frac{\delta}{2} + \frac{dG}{dn'} \right) \phi \\ = -D_1(M)u^{inc}(M) - q_1 N_1(M) \frac{du^{inc}}{dn}(M) \end{aligned} \quad (68)$$

with

$$\begin{aligned} N_1(M) &= \int_{-\infty}^{+\infty} G_1(M, M') dx' \\ &\approx \frac{-i}{4k_1} \frac{1}{\sqrt{1 + \xi'^2(x)}} \end{aligned} \quad (69)$$

$$\begin{aligned} D_1(M) &= \int_{-\infty}^{+\infty} \left( \frac{\delta}{2} - \frac{dG_1}{dn'} \right) (M, M') dx' \\ &\approx \frac{1}{2} - \frac{i}{4k_1} \frac{\xi''}{(x)} \sqrt{1 + \xi'^2(x)}, \end{aligned} \quad (70)$$

where  $\xi'$  and  $\xi''$  denote the first and second derivatives of the surface profile.

The numerical implementation requires a sampling in the Fourier space of the unknown surface density  $\phi$ . With the aim of using FFT algorithms, the unknown is assumed to be periodic, with periodicity  $L$  equal to the length of the sampled interval, to make

sure this periodicity has no influence on the result. In other words, the surface density coincides with the periodic computed unknown on  $[-L/2, L/2]$  and vanishes outside.

Denoting by

$$\tilde{f}_n = \frac{1}{L} \int_{-L/2}^{L/2} f(x') \exp(2i\pi n x' / L) dx'$$

the  $n$ th Fourier coefficient of a function  $f(x)$  and by  $f_m = \int_{-\infty}^{+\infty} f(x) t_m(x) dx$  the scalar product of  $f$  with a test function  $t_m$ , the discretised form of the integral equation (68) writes

$$D_{1m} \sum_n A_{m,n} \tilde{\phi}_n + q_1 N_{1m} \sum_n B_{m,n} \tilde{\phi}_n = -D_{1m} u_m^{\text{inc}} - q_1 N_{1m}(M) \left( \frac{du^{\text{inc}}}{dn} \right)_m \quad (71)$$

with

$$A_{m,n} = \frac{1}{L} \int_{x=-\infty}^{+\infty} \int_{x'=-L/2}^{L/2} G(x, x') t_m(x) \times \exp(2i\pi n x' / L) dx dx' \quad (72)$$

$$B_{m,n} = \frac{1}{2} (\tilde{t}_m)_n + \frac{1}{L} \int_{x=-\infty}^{+\infty} \int_{x'=-L/2}^{L/2} \frac{dG}{dn}(x, x') t_m(x) \times \exp(2i\pi n x' / L) dx dx'. \quad (73)$$

For accurate computation of the matrix elements from Eqs. (72) and (73), the choice of the test functions  $t_m$  must obey the same constraints as in a classical method of moments, typically 10 sampling points per wavelength in the resonance domain, but here, this does not influence the number of unknowns, resulting from the truncation of the Fourier series in Eq. (71).

To validate and show the capabilities of the method, we have compared numerical results with the experimental results described in West and O'Donnell (1995). An interface separating air from gold is illuminated in the visible region ( $\lambda_0 = 0.612 \mu\text{m}$ ,  $\epsilon_1 = -9.1 + i1.1$ ). The spectral density  $S(K)$  is a window function centred at  $K = 2\pi/0.578 \mu\text{m}^{-1}$  and width  $\Delta K = 2\pi/1.315 \mu\text{m}^{-1}$ . The rms height of the surface is rather small:  $\sigma = 0.0109 \mu\text{m}$ . In Fig. 11, we have plotted the surface density  $\phi(x)$  when the surface is illuminated by a beam of width  $w = 18\lambda_0$ . The strong excitation of the surface waves leads to a low decay of the surface density that needs about 100 wavelengths to become negligible. To solve this problem accurately, 2200 test functions but only 1200 Fourier coefficients for  $\phi$  were needed. Compared to a method of moments, the number of unknowns is thus divided by a fac-

tor close to 2. The scattering pattern shown in Fig. 12 agrees very well with that of Fig. 7 of West and O'Donnell (1995), and exhibits a strong *backscattering enhancement* as a result of multiple scattering of surface waves.

### Scattering by Rough Inhomogeneous Media

Now, the lower medium is no longer homogeneous but contains bounded scatterers, and we focus on the statistical problem with many small homogeneous scatterers uniformly distributed (Fig. 13).

**Limitation of Integral Methods** Since all the scatterers are homogeneous, the boundary integral method described above can be generalised easily. However, as a strong shortcoming, when the number of embedded scatterers is increased, both memory and computation time requirements also increase very rapidly. For instance, a small cylindrical scatterer requires at least 10 boundary finite elements, and the singularity of the kernels of the integral equation must be treated carefully. On the other hand, the scattered field can be accurately described with a small number of terms in the Fourier–Bessel expansion: only one for  $s$ -polarisation (isotropic scattering) and three for  $p$ -polarisation. Therefore, we have developed an hybrid method, where a mixed representation of the scattered field is used: an integral representation for the contribution from the surface density lying on the rough interface, and a Fourier–Bessel expansion for the volume scattering part (see §3). This approach drastically reduces the number of unknowns, at least in the case of scatterers with dimensions smaller than the wavelength. As a counterpart, a rigorous treatment requires the calculation of the scattering matrix of the object. This goal can be achieved with the help of the method of fictitious sources described in the second section of this chapter.

### Combination of Integral and S Matrix Formalisms

Let us consider a set of homogeneous scatterers  $\Omega_j (j \geq 1)$  bounded by  $\mathcal{C}_j$ , and an associated set of local systems of coordinates  $O_j xy$ , with the origin  $O_j$  located inside  $\Omega_j$ . The local polar coordinates of a point  $P$  are given by  $r_j = O_j P$  and  $\theta_j = (O_j x, O_j P)$ . Let us denote by  $u_j^{\text{sc}}$  the Fourier–Bessel expansion of the field scattered by the  $j$ th rod in terms of outgoing Hankel functions

$$u_j^{\text{sc}}(P) = \sum_{n=-\infty}^{+\infty} b_{j,n} H_n^{(1)}(k_1 r_j) \exp(in\theta_j), \quad (74)$$

where  $k_1$  represents the wavenumber in the surrounding medium. This expression is valid outside the smallest circle centred at  $O_j$  containing  $\Omega_j$ . If the Bessel functions are chosen for the description of the

**Figure 11** Modulus of the surface density (solid line) and of the incident magnetic field (dashed line) versus  $x(\mu\text{m})$ , on a gold-coated rough surface illuminated by a p-polarised Gaussian beam with wavelength  $\lambda = 0.612 \mu\text{m}$ .

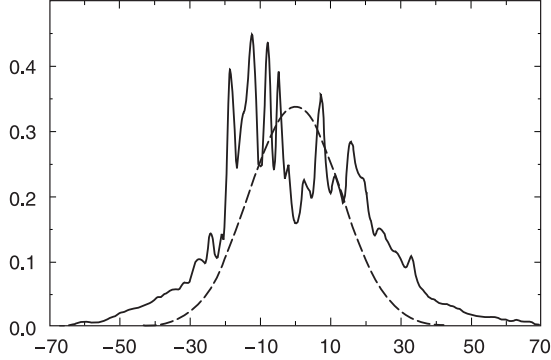
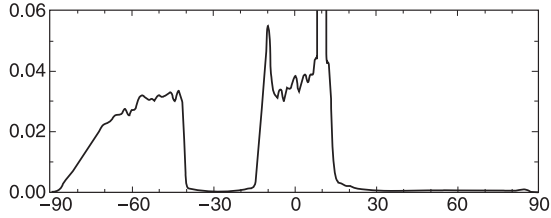


**Figure 12** Differential reflection coefficient versus scattering angle  $\Theta^{\text{sc}}$ , averaged over 500 samples illuminated by a Gaussian beam ( $w = 18\lambda$ ,  $\Theta^{\text{inc}} = 10^\circ$ ). The backscattering peak is located at  $-10^\circ$ , and the specularly reflected beam at  $10^\circ$  has been truncated.



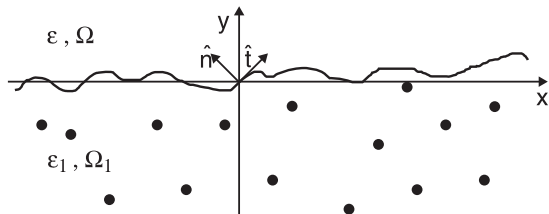
field  $u_j^{\text{imp}}$  impinging on the  $j$ th rod, we have

$$u_j^{\text{imp}}(r_j, \theta_j) = \sum_{m=-\infty}^{+\infty} a_{j,m} J_m(k_1 r_j) \exp(im\theta_j), \quad (75)$$

where the incident and scattered complex amplitudes,  $a_{j,m}$  and  $b_{j,n}$  respectively, are linked through the scattering matrix  $S_j$ . Still using a boundary integral representation for surface scattering, Eq. (63) becomes, at any point on  $\mathcal{C}$ ,

$$\left[ \left( \frac{\delta}{2} - \frac{dG_1}{dn'} \right) G + q_1 G_1 \left( \frac{\delta}{2} + \frac{dG}{dn'} \right) \right] \phi + \sum_{j \geq 1} u_j^{\text{sc}}$$

**Figure 13** Geometry of the surface–volume scattering problem. A set of homogeneous rods is embedded in the lower medium, below a rough interface.



$$= -\left( \frac{\delta}{2} - \frac{dG_1}{dn'} \right) u^{\text{inc}} - q_1 G_1 \frac{du^{\text{inc}}}{dn}. \quad (76)$$

This equation gives a first set of relationships, that couples the surface density  $\phi$  and the incident amplitudes  $a_{j,n}$ . To complete the linear system, we must link  $a_{j,n}$  to the field radiated by the surface density and by the other rods toward the  $j$ th rod. The first step consists in projecting this field onto the local basis of incident fields  $J_n(k_1 r_j) \exp(in\theta_j)$ . Let  $P(r_j, \theta_j)$  be a point in the neighbourhood of  $O_j$ , and  $M'(r'_j, \theta'_j)$  a point on the surface  $\mathcal{C}$ . Thanks to Graf's formula, if  $O_j P < O_j M'$ ,

$$G_1(P, M') = \frac{-i}{4} \sum_{m=-\infty}^{+\infty} H_m^{(1)}(k_1 r'_j) \times J_m(k_1 r_j) \exp(im(\theta_j - \theta'_j)), \quad (77)$$

$$\hat{\mathbf{n}}' \cdot \text{grad}_{M'} G_1(P, M') = \frac{-i}{4} \sum_{m=-\infty}^{+\infty} C_m(M') \times J_m(k_1 r_j) \exp(im(\theta_j - \theta'_j)) \quad (78)$$

with

$$C_m(M') = \frac{\partial H_m^{(1)}(k_1 r'_j)}{\partial r'} \frac{\hat{\mathbf{n}}' \cdot \mathbf{O}_j M'}{r'_j} - \frac{im}{r'_j} H_m^{(1)}(k_1 r'_j) \frac{\hat{\mathbf{r}}' \cdot \mathbf{O}_j M'}{r'_j}. \quad (79)$$

Then the field radiated in  $P$  by the surface density  $\phi$  writes

$$u_{\text{surf}}^{\text{sc}}(P) = \sum_{m=-\infty}^{+\infty} a_{j,m}^{(s)} J_m(k_1 r_j) \exp(im\theta_j) \quad (80)$$

with

$$a_{j,m}^{(s)} = \frac{-i}{4} \int_{\mathcal{C}} [C_m(M') u(M') - H_m^{(1)}(k_1 O_j M') \left( \frac{du}{dn'} \right)_{\Omega_1}(M')] ds', \quad (81)$$

where  $u(M')$  and its normal derivative are given by Eqs. (61) and (62). Hence, Eq. (81) allows us to express the incident amplitudes as a function of the surface density. The same projection is also applied to the field scattered by the other rods toward  $\Omega_j$ , as explained in the previous section. Applying Eqs. (35) and (36) and adding the surface contribution leads to

$$a_{j,m} = a_{j,m}^{(s)} + \sum_{l \neq j} \sum_{n=-\infty}^{+\infty} \sum_{p=-\infty}^{+\infty} S_{l,np} a_{l,p} \times H_{m-n}^{(1)}(k_1 O_l O_j) \exp(i(n-m)\theta_l(O_j)). \quad (82)$$

Therefore, provided the scattering matrix is known for each rod, Eqs. (76) and (82) lead to a set of linear equations with incident amplitudes  $a_{l,p}$  and surface density  $\phi$  as unknowns, with the same number of equations and unknowns.

**Numerical Results** This method has been used to investigate the possibility of separating this surface–

volume scattering problem into two simpler problems, surface scattering and a volume scattering, the scattering patterns then being added incoherently. Such a conjecture is suggested by some approximate theories (Calvo-Perez *et al.*, 1999), but the domain of validity of this rule is not known, and only a rigorous tool can investigate strong roughness, high dielectric contrast, high density of scatterers, etc.

Let us consider a Gaussian rough surface with rms height  $\sigma = 0.3\lambda_0$  and correlation length  $l = \lambda_0/2$  (length such that  $C(l)/C(0) = 1/e$ ), separating vacuum from a lossy medium with permittivity  $\epsilon_1 = 3 + i0.4$ , in which small perfectly conducting circular rods (radius  $a = 0.07\lambda_0$ ) are filling 3% of the volume. The incident beam is  $s$ -polarised with waist  $6\lambda_0$  and mean incident angle  $\Theta^{\text{inc}} = 20^\circ$ . In this problem, a few hundreds of rods lie in each sample, and thanks to this method the number of unknowns is restricted to about 1500. Figure 14 shows the scattering pattern at infinity (solid line), and compares it with that obtained by summing two contributions (dashed line):

(i) the intensity scattered from a rough surface with the same geometrical parameters, but effective permittivity derived from Keller effective medium theory (dotted line) (Keller, 1964) and

(ii) the intensity scattered from the metallic rods below a flat interface (dot-dashed line).

It must be noted that the patterns agree amazingly well except in the specular and backscattering directions.

In conclusion, the computational efficiency of this method comes from the combination of natural bases

for bounded and unbounded scatterers: cylindrical harmonics on one hand, boundary finite elements on the other. In addition, thanks to the beam simulation method, samples with arbitrary size can be handled. Therefore, it is a very versatile tool for investigating scattering properties of inhomogeneous coatings like paints or studying phenomena like backscattering enhancement or the shift of Brewster's angle due to disorder.

## §5. Conclusion

We have presented numerical methods of increasing complexity that are able to solve with precision a wide variety of problems of scattering, including scattering from a single object, scattering by a set of randomly or periodically placed scattering objects and scattering by an arbitrary set of scatterers located below a random interface separating two dielectric materials.

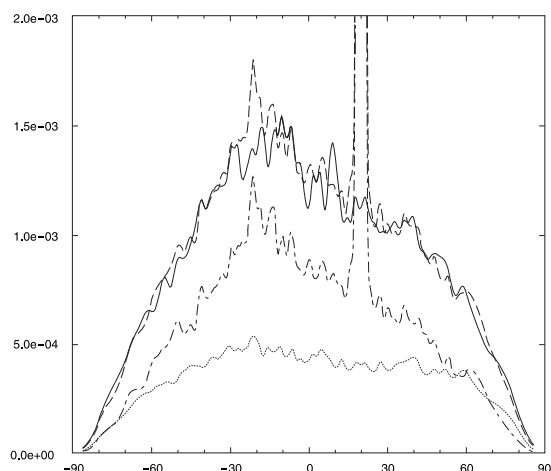
The same kinds of problem may be solved using well-known methods like boundary or volume finite-elements methods and FDTD, but it appears that the methods we have described are very efficient and attractive in many practical problems.

A generalisation of these methods to 3D problems of scattering is straightforward from a pure theoretical viewpoint, but very costly for the numerical implementation. It is worth noting that some of these generalisations have been achieved, for instance the use of fictitious sources method for 3D scatterers (Hafner, 1990), the use of the S-matrix method for a set of spheres (Defos du Rau, 1997) and the use of the one-unknown integral equation for scattering from randomly rough surfaces (Pak *et al.*, 1997). Of course, the numerical programs are much more difficult to implement than those devoted to 2D objects but progress in the modelling of 3D objects is necessary for many practical applications like the study of doped or nondoped photonic crystals, precise treatment of sea or ground scattering and remote sensing for buried objects.

## References

- Abramovitz, M. and Stegun, I. 1970, *Handbook of Mathematical Functions*. Dover, New York.
- Boag, A., Leviatan, Y. and Boag, A. 1988, Analysis of two-dimensional electromagnetic scattering from a periodic grating of cylinders using a hybrid current model. *Radio Sci.* **23**, 612–624.
- Boag, A., Leviatan, Y. and Boag, A. 1989, Analysis of diffraction from echelette gratings, using a strip-current model. *J. Opt. Soc. Am. A* **6**, 543–549.
- Boag, A., Leviatan, Y. and Boag, A. 1993, Analysis of electromagnetic scattering from doubly-periodic nonplanar

**Figure 14** Differential reflection coefficients versus scattering angle  $\Theta^{\text{sc}}$ , averaged over 400 samples illuminated by a Gaussian beam ( $w = 6\lambda$ ,  $\Theta^{\text{inc}} = 20^\circ$ ). Solid line: scattering from the rough inhomogeneous medium. Dot-dashed line: scattering from the rods below a flat interface. Dotted line: scattering from a rough surface with effective lower medium. Dashed line: sum of the last two curves.



- surfaces using a patch-current model. *IEEE Trans. Ant. Prop.* **41**, 732–738.
- Brown, G. 1998, Guest editorial: Special Issue on Low-Grazing-Angle Backscatter from Rough Surfaces. *IEEE Trans. Ant. Prop.* **46**, 1.
- Cadilhac, M. and Petit, R. 1992, On the diffraction problem in electromagnetic theory: A discussion based on concepts of functional analysis including an example of practical application. In *Huyghens' Principle 1690–1990, Theory and Applications* (H. Block, H. A. Ferwerda and H. K. Kuiken, Eds.), pp. 249–272. Elsevier, Amsterdam.
- Calvo-Perez, O., Sentenac, A. and Greffet, J. J. 1999, Light scattering by a two-dimensional rough penetrable medium: A mean field theory. *Radio Sci.* **34**, 311–335.
- Chew, W. C., Gürel, L., Wang, Y. M., Otto, G., Wagner, R. L. and Liu, Q. H. 1992, A generalized recursive algorithm for wave-scattering solutions in two dimensions. *IEEE Trans. Microwave Theory Tech.* **40**, 716–723.
- Colton, D. and Kress, R. 1983, *Integral Equations Methods in Scattering Theory*. Wiley, New York.
- Dailant, J. and Gibaud, A. 1999, *Xray and Neutron Reflectivity: Principles and Applications*, Lectures Notes in Physics. Springer-Verlag, Heidelberg.
- Defos du Rau, M. 1997, Thesis, University of Bordeaux.
- Elsherbeni, A. Z. and Kishk, A. A. 1992, Modeling of cylindrical objects by circular dielectric and conducting cylinders. *IEEE Trans. Ant. Prop.* **40**, 96–99.
- Felbacq, D., Tayeb, G. and Maystre, D. 1994, Scattering by a random set of parallel cylinders. *J. Opt. Soc. Am. A* **11**, 2526–2538.
- Goodman, J. W. 1975, *Laser Speckle and Related Phenomena*, Topics in Applied Physics. Springer-Verlag, New York.
- Hafner, C. 1990, *The Generalized Multipole Technique for Computational Electromagnetics*. Artech House Books, Boston.
- Hafner, C. 1995, Multiple multipole program computation of periodic structures. *J. Opt. Soc. Am. A* **12**, 1057–1067.
- Hastings, F. D., Schneider, J. B. and Broschat, S. L. 1995, A monte Carlo FDTD technique for rough surface scattering. *IEEE Trans. Ant. Prop.* **43**, 1183–1191.
- Joannopoulos, J., Meade, R. and Winn, J. 1995, *Photonic Crystals*. Princeton Univ. Press, Princeton, NJ.
- Keller, J. B. 1964, Stochastic equations and wave propagation in random media. *Proc Symp. Appl. Math.* **16**, 145–170.
- Kupraze, V.D. 1967, On the approximate solutions of problems in mathematical physics. *Russ. Math. Surveys* **22**, 58–108.
- Leviatan, Y. and Boag, A. (1987) Analysis of electromagnetic scattering from dielectric cylinders using a multifilament current model. *IEEE Trans. Ant. Prop.* **35**, 1119–1127.
- Lord Rayleigh 1892, On the influence of obstacles arranged in rectangular order upon the properties of a medium. *Phil. Mag.* **34**, 481–502.
- Maradudin, A. A., Mendez, E. R. and Michel, T. 1989, Backscattering effects in the elastic scattering of p-polarized light from a large-amplitude random metallic grating. *Opt. Lett.* **14**, 151–153.
- Martin, P. A. and Ola, P. 1993, Boundary integral equations for the scattering of electromagnetic waves by a homogeneous dielectric obstacle. *Proc R. Soc. Edinburgh A* **123**, 185–208.
- Marvin, A. M. and Celli, V. 1994, Relation between the surface impedance and the extinction theorem on a rough surface. *Phys. Rev. B* **50**, 14,546–14,553.
- Maystre, D. 1983, Electromagnetic scattering from perfectly conducting rough surfaces in the resonance region. *IEEE Trans. Ant. Prop.* **31**, 885–895.
- Maystre, D. 1994, Electromagnetic study of photonic band gaps. *Pure Appl. Opt.* **3**, 975–993.
- Maystre, D. and Saillard, M. 1994, Localization of light by randomly rough surfaces: Concept of localiton. *J. Opt. Soc. Am. A* **11**, 680–690.
- Maystre, D. and Vincent, P. 1972, Diffraction d'une onde électromagnétique plane par un objet cylindrique non infiniment conducteur de section arbitraire. *Opt. Comm.* **5**, 327–330.
- Nicorovici, N. A., McPhedran, R. C. and Botten, L. C. 1995, Photonic band gaps for arrays of perfectly conducting cylinders. *Phys. Rev. E* **52**, 1135–1145.
- Pak, K., Tsang, L. and Johnson, J. 1997, Numerical simulations and backscattering enhancement of electromagnetic waves from two-dimensional dielectric random rough surfaces with the Sparse Matrix Canonical Grid method. *J. Opt. Soc. Am. A* **14**, 1515–1529.
- Petit, R. and Zolla, F. 1994, The method of fictitious sources as applied to the conical diffraction by a homogeneous rod. *J. Electr. Waves Appl.* **8**, 1–18.
- Saillard, M. and De Santo, J. A. 1996, A coordinate-spectral method for rough surface scattering. *Waves Random Media* **6**, 135–150.
- Saillard, M. and Maystre, D. 1988, Scattering from random rough surfaces: A beam simulation method. *J. Opt.* **19**, 173–176.
- Saillard, M. and Maystre, D. 1990, Scattering from metallic and dielectric rough surfaces. *J. Opt. Soc. Am. A* **7**, 982–990.
- Soto-Crespo, J. M. and Nieto-Vesperinas, M. 1989, Electromagnetic scattering from very rough random surfaces and deep reflection gratings. *J. Opt. Soc. Am. A* **6**, 367–384.
- Suratteau, J. Y. and Petit, R. 1984, The electromagnetic theory of the infinitely conducting wire grating using a Fourier-Bessel expansion of the field. *Internat. J. Infrared millimeter waves* **5**, 1189–1200.
- Tayeb, G. 1990, Thesis, University of Aix-Marseille III.

- Tayeb, G. 1994, The method of fictitious sources applied to diffraction gratings. *Appl. Comput. Electromagnetics Soc. J.* **9**, 90–100.
- Tayeb, G. and Maystre, D. 1997, Rigorous theoretical study of finite-size two-dimensional photonic crystals doped by microcavities. *J. Opt. Soc. Am. A* **14**, 3323–3332.
- Tayeb, G., Petit, R. and Cadilhac, M. 1991, The synthesis method applied to the problem of diffraction by gratings: The method of fictitious sources. *Internat. Conf. Appl. Theory Periodic Structures SPIE 1545*, 95–105.
- Torrance, K. E. and Sparrow, E. M. 1967, Theory of off-specular reflection from roughened surfaces. *J. Opt. Soc. Am.* **57**, 1105–1114.
- Tsang, L., Kong, J. A. and Shin, R. T. 1985, *Theory of Microwave Remote Sensing*. Wiley Series in Remote Sensing, Wiley, New York.
- Van Bladel, J. 1964, *Electromagnetic Fields*. McGraw-Hill, New York.
- Vlassis, M., McPhedran, R. C. and Nicorovici, N. A. 1996, Radiation modes of multiple core fibres. *Opt. Comm.* **129**, 256–272.
- West, C. S. and O'Donnell, K. A. 1995, Observations of backscattering enhancement from polaritons on a rough metal surface. *J. Opt. Soc. Am. A* **12**, 390–397.
- Wood, R. W. 1902, On a remarkable case of uneven distribution of light in a diffraction grating spectrum. *Phil. Mag.* **4**, 396–402.
- Yablonovitch, E. 1994, Photonic crystals. *J. Modern Opt.* **41**, 173–194.
- Youssif, H. A. and Köhler, S. 1988, Scattering by two penetrable cylinders at oblique incidence. I. The analytical solution. *J. Opt. Soc. Am. A* **5**, 1085–1096.
- Zolla, F. 1993, Thesis, University of Aix-Marseille III.
- Zolla, F. and Petit, R. 1996, Method of fictitious sources as applied to the electromagnetic diffraction of a plane wave by a grating in conical diffraction mounts. *J. Opt. Soc. Am. A* **13**, 796–802.
- Zolla, F., Petit, R. and Cadilhac, M. 1994, Electromagnetic theory of diffraction by a system of parallel rods: The method of fictitious sources. *J. Opt. Soc. Am. A* **11**, 1087–1096.